

# Dimensionality Reduction and Motion Clustering during Activities of Daily Living: 3, 4, and 7 Degree-of-Freedom Arm Movements

Yuri Gloumakov, *Student Member, IEEE*, Adam J. Spiers, *Member, IEEE*, and Aaron M. Dollar, *Senior Member, IEEE*

**Abstract**—This paper is the first in a two-part series analyzing human arm and hand motion during a wide range of unstructured tasks. The wide variety of motions performed by the human arm during daily tasks makes it desirable to find representative subsets to reduce the dimensionality of these movements for a variety of applications, including the design and control of robotic and prosthetic devices. This paper presents a novel method and the results of an extensive human subjects study to obtain representative arm joint angle trajectories that span naturalistic motions during Activities of Daily Living (ADLs). In particular, we seek to identify sets of useful motion trajectories of the upper limb that are functions of a single variable, allowing, for instance, an entire prosthetic or robotic arm to be controlled with a single input from a user, along with a means to select between motions for different tasks. Data driven approaches are used to discover clusters and representative motion averages for the wrist 3 degree of freedom (DOF), elbow-wrist 4 DOF, and full-arm 7 DOF motions. The proposed method makes use of well-known techniques such as dynamic time warping (DTW) to obtain a divergence measure between motion segments, Ward’s distance criterion to build hierarchical trees, and functional principal component analysis (fPCA) to evaluate cluster variability. The emerging clusters associate various recorded motions into primarily hand start and end location for the full-arm system, motion direction for the wrist-only system, and an intermediate between the two qualities for the elbow-wrist system.

**Index Terms**—Hierarchical clustering, manipulation, motion analysis, upper limb, prosthetics, robotics.

## I. INTRODUCTION

THE human arm is a remarkable tool that enables us to complete a wide range of complex manipulation tasks. Unlike gait, the arm regularly performs seemingly complex and varied motions [1], [2]. Despite that, there appears to be some degree of regularity that does not impose much cognitive burden [3], [4]. We therefore predict that the spectrum of arm motions can be distilled to a small subset of motion models, for example, by using unsupervised learning techniques. Data driven clustering approaches are explored and implemented to

This work was submitted on May 5, 2020 for review. This work was supported by the Congressionally-Directed Medical Research Programs (CDMRP) under grant- W81XWH-15-10407. The work presented in this paper is an expansion of the authors’ previous work found in [23].

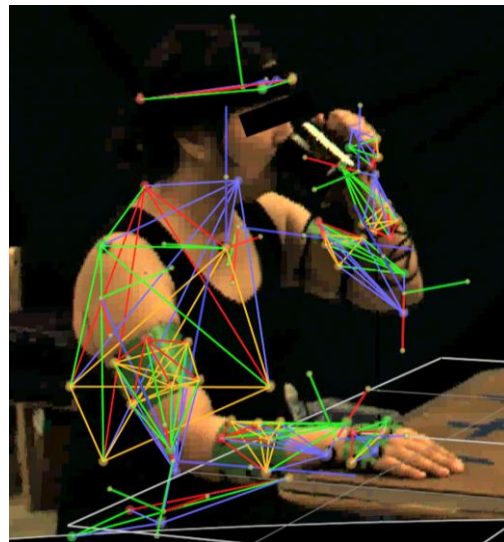


Fig. 1. Subject performing an ADL task, drinking from a mug. The subject’s motion capture ‘skeleton’ is superimposed in this image. Redundant markers are included to enable the prediction of occluded marker locations and maintain the ability to identify joint centers.

identify underlying groupings of 3 degree-of-freedom (DOF), 4 DOF, and 7 DOF joint angle trajectories of the wrist, elbow-wrist, and shoulder-elbow wrist, respectively, of the upper limb (hereafter simply referred to as “arm motions”) from healthy individuals performing a selected set of activities of daily living (ADL). Clustering is a knowledge discovery approach that quantitatively builds a categorization model, as opposed to training a classifier with pre-labeled data, and would therefore be most appropriate at identifying motion categories that could be quantitatively validated. We ultimately seek to find relatively small sets of “useful” arm motion trajectories that are functions of a single variable. This approach would, for instance, allow an upper-limb amputee to control a multi-DOF prosthetic arm using a single control input, such as from two-site EMG, which is the current standard in clinical practice [5].

Reduced dimensionality representation of upper-limb movements can be useful in a variety of domains, including operating a semi-autonomous prosthetic device by combining

Y. Gloumakov and A.M. Dollar are with the Mechanical Engineering and Materials Science Department, Yale University, New Haven, CT 06511 USA, (email: {yuri.gloumakov, aaron.dollar} @yale.edu).

A.J. Spiers is with the Max Planck Institute for Intelligent Systems, Stuttgart, 70597, Germany (email: a.spiers@is.mpg.de).

series of sub-motions to accomplish a larger set of tasks. Research groups investigating control of active prosthetic wrists and elbows have previously used joint synergies while primarily focusing on a single sub-motion, namely reaching [6], [7]. Our methodology aims not to only validate reaching as a unique motion category, but also stratify all sub-motions to a hierarchical structure and formalize the sub-motion categories, including manipulation. This work enables future efforts to take advantage of and focus on demonstrable categories of motion.

Due to the large variety of motions that the human arm can achieve, it was important to focus our clustering efforts on motions that are relevant to daily life, i.e. common tasks related to ADLs (Fig. 1). The selected tasks that were included in the present work were largely inspired by standardized ‘outcome measure’ assessment tools of arm function, such as AM-ULA [8], and reports that surveyed motion-impaired participants regarding which tasks they prioritize [9]–[11]. The identified tasks were crucial for independent living, and included food preparation, hygiene, dressing, grooming, and eating; none of which are considered physically challenging.

Previous research efforts on upper limb motion have spanned various disciplines and techniques aimed at gaining insight into how humans make use of and control their upper limbs. Research methods have included neural networks, non-linear control, and musculoskeletal modelling [12]. Some investigations have attempted to control upper-limb prosthetic devices by identifying and making use of underlying healthy motion patterns [13], [14]. These include performing pattern recognition of simultaneous motion primitives [15] or using artificial neural networks to discriminate or predict upper-limb functions [7], [16] in healthy participants. Other groups extracted subsets of arm motion primitives from healthy participants using functional principal component analysis (fPCA) [17]–[19]. Instead of using a linear combination of movement primitives to perform a complete task, a more straightforward approach to controlling an upper-limb device could instead be made up of a sequence of individual sub-motions, as is proposed in this paper. Hierarchical description and on-line motion recognition of non-ADL motion segments have been performed in [20]. However, efforts were on creating non deterministic automatic motion recognition technology of whole body motions rather than on sequential motion segments. Other relevant fields, including rehabilitation, have analyzed the ranges of joint angles as a measure of healthy motion patterns [2], [21], [22]. Although efforts have been made to extract underlying motion patterns [7], [17], [20], none have deterministically stratified arm motions related to ADLs.

This paper is an extension of a previous conference paper by the authors [23], and expands and extends it in a number of ways. The changes are as follows: (a) 3 (wrist) and 4 (elbow-wrist) DOF cases are analyzed in addition to 7 DOF for application in technologies assisting patients with different degrees of arm disability or amputation, (b) 4 DOF (shoulder-elbow) trajectories are examined to verify the location-dominant cluster characteristics of the 7 DOF model found in the previous work, (c) an increased number of subjects (from 5 to 12), (d) a set of motion modalities are established for each

DOF model, (e) variabilities of motion within each of the clusters are identified using fPCA, and (f) results are demonstrated using accompanying animations visually reassuring their use in real-world applications.

## II. EXPERIMENT PROTOCOL

### A. Task Protocol

In this study we asked healthy participants to perform set of tasks related to daily life. Standard function measure AM-ULA [8], was used to identify the set of tasks, which are listed in Table 1 along with task specifications in Fig. 2. Only a subset of AM-ULA tasks were included that had identifiable start and end points, such that complex motions that occurred during a task could be segmented into distinct motion segments. For example, the drinking task involves distinct sub-motions such as reaching, drinking, and returning the cup to the table. Tasks that lacked distinct motion segments were omitted and include folding a towel or donning a shirt. Omitted tasks also include small amplitude cyclical tasks, such as stirring with a spoon or cutting with a knife.

The protocol was completed by 12 (6 male, 6 female) healthy participants, chosen to uniformly span the age groups of 20-70 so as to make the motion analysis results as generalizable as possible (also for prosthesis application); this resulted in a final

TABLE I  
TASKS AND CORRESPONDING MOTION SEGMENTS

Task Code	Standing Tasks <sup>a</sup>
t2b	(1) reach box on top shelf (2) move box to bottom (3) return hands
b2t	(1) reach box on bottom shelf (2) move box to top (3) return hands
t2m	(1) reach box on top shelf (2) move box to mid (3) return hands
m2t	(1) reach box on mid shelf (2) move box to top (3) return hands
m2b	(1) reach box on mid shelf (2) move box to bottom (3) return hands
b2m	(1) reach box on bottom shelf (2) move box to mid (3) return hands
ke	(1) bring key to keyhole (2) turn key (3) turn back (4) remove key from keyhole and return hand
kn	(1) reach for door knob (2) turn knob (3) turn back (4) return hand
dh	(1) reach for door handle (2) open door (3) return hand
oh	(1) reach for can on top shelf (2) bring can down in front of the body
mp	(1) reach for mug in C1 (2) take a sip (3) return mug (4) return hand
md	(1) reach for mug in C2 (2) take a sip (3) return mug (4) return hand
mc	(1) reach for mug in C3 (2) take a sip (3) return mug (4) return hand
cp	(1) reach for cup in C1 (2) take a sip (3) return mug (4) return hand
cd	(1) reach for cup in C2 (2) take a sip (3) return mug (4) return hand
cc	(1) reach for cup in C3 (2) take a sip (3) return mug (4) return hand
st	(1) reach for suitcase (2) transfer suitcase to table (3) return hands
ax	(1) bring hand to contralateral axilla (2) return hand
pt	(1) bring hand to back pocket (2) return hand
Sitting tasks <sup>a</sup>	
sp	(1) reach for spoon (2) bring spoon to bowl (3) scoop (4) bring to mouth (5) return spoon (6) return hand
fr	(1) reach for fork (2) stab the middle of the plate (3) bring to mouth (4) return fork (5) return hand
ms	(1) reach for mug (2) take a sip (3) return mug (4) return hand
cs	(1) reach for cup (2) take a sip (3) return cup (4) return hand
pr	(1) reach for cup (2) pour (3) return cup (4) return hand

<sup>a</sup>Unless otherwise specified, standing tasks started and ended with the subjects’ hands by their side while for sitting tasks the hands were to start and end on the table palm side down.

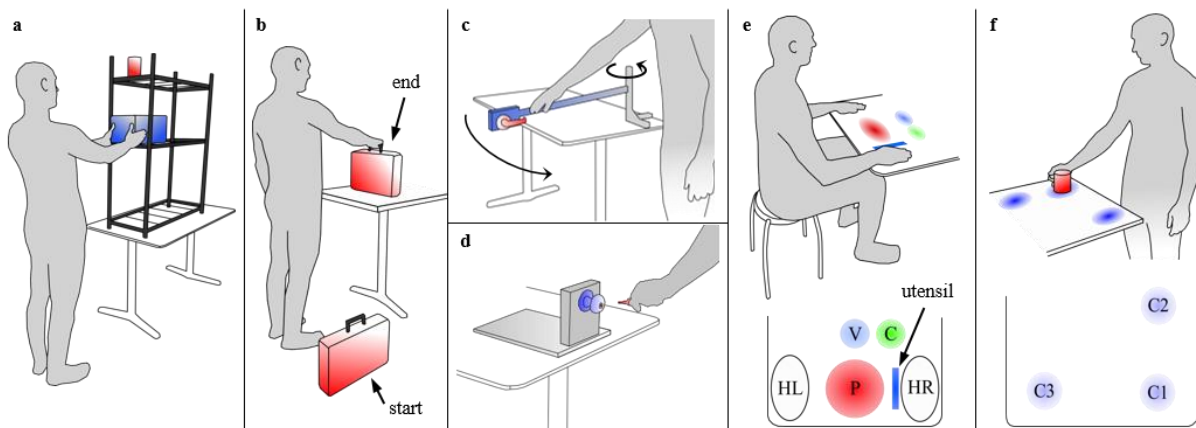


Fig. 2. Depictions of several selected protocol tasks: (a) a box object was to be moved from one specified shelf to another. The object on the top shelf is the location of the can during overhead reaching tasks. (b) The initial and final locations of the suitcase tasks, (c) simulated door opening task, and (d) simulated door knob and key tasks. (e) The set up for the sitting tasks: the left and right hand start and end in HL and HR, a utensil is placed next to HR, a bowl or plate are placed in P, a cup or mug is placed in C, and a container to collect the water during the pouring task is placed in V. (f) The three target locations of the standing cup and mug tasks, during which the table is elevated to simulate a countertop, where C2 is 25 cm from C1 and C3 is 45 cm from C1. The task conditions for left handed participants are mirrored. Table height is 74 cm, and is elevated to 92 cm to simulate a counter top for the standing cup and mug tasks. The mug (9.5 cm height, 8 cm diameter), can (7.5 cm height, cm diameter), box (21x37x19 cm), and suitcase (43x9x30 cm) weigh 0.36, 0.09, 0.23, and 1.36 kg respectively. The shelves are 80, 140, and 180 cm above the floor. Door knob and handle are 90 cm above the floor, and the simulated door swivels with an 84 cm radius.

age range of 24 to 71, mean of 43, and standard deviation of 15. Participants performed 24 individual tasks over the course of a single 5 hour visit. Although many breaks were included throughout the experiment to further avoid physical and mental fatigue, such as between tasks, participants were given as many additional breaks as they requested; most opted out, but some took one or two additional 5 minute breaks. Each task was repeated 3 times, providing a way to average and smooth the motions as well as account for outliers during analysis. The 24 tasks were segmented to 2 to 6 motion segments, yielding 85 distinct motion segments per participant. Participants were instructed to begin and end each task in predefined ‘rest poses’; hands by the side of the body for standing tasks and with the palms on the table for sitting tasks. Minimal instruction was given on how the tasks should be completed. Experimental set-up was inverted for left-handed participants.

This study protocol was approved by Yale University Institutional Review Board, HSC# 1610018511.

### B. Data Acquisition

Arm motions were recorded with Vicon Motion Capture System (Oxford Metrics Limited, Oxford) using 12 infrared ‘Bonita’ model cameras (100 frames/second), 1 video reference camera, and 55 reflective markers placed on the body. The video camera was synchronized with the motion capture

cameras and was used to help with marker identification within the Nexus software.

### III. DATA ANALYSIS

The goal is to identify how upper-limb motions related to ADL cluster and obtain a subset of representative motions using data driven approaches. The data processing and analysis pipeline is illustrated in Fig. 3. The motion data is first converted to joint angle trajectories and manually segmented into sequential reaching and manipulation movements. Each sub-movement is then averaged across repetitions. A distance matrix is created and used for clustering. Clusters are evaluated twice: first to decide on the number of clusters, then against alternative algorithms. Finally, representative motions are obtained from each cluster and their respective variances are computed. Since the 4 DOF shoulder-elbow system was included solely to compare against the 7 DOF system, this portion of the analysis is limited to only obtaining the clusters.

#### A. Motion Representation

Recorded human arm motion data can be represented in different ways, such as joint angles of the shoulder, elbow, and wrist, or Cartesian coordinates of the arm segments. Although the joint angle method suffers from the unequal impact that different joints have on the end effector trajectory, fewer

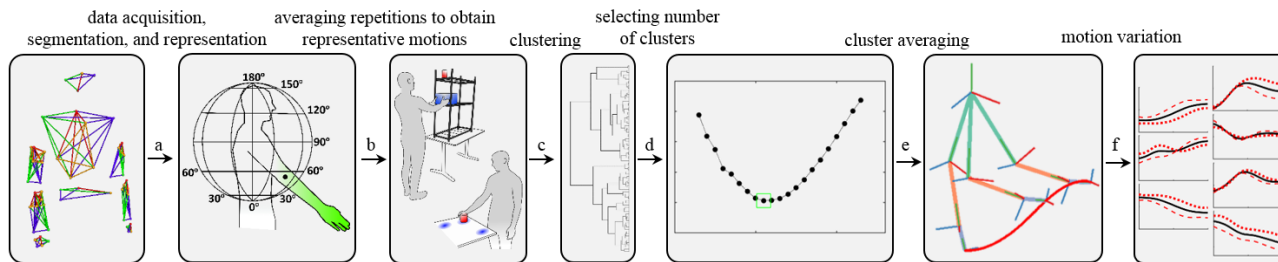


Fig. 3. General framework of the data processing and analysis. (a) Cartesian coordinates of markers tracking human motion are converted to arm joint angles, creating a set of feature variables generalizable across subjects. (b) Repetitions of different motions and subjects are segmented and averaged. (c) The motions are compared using DTW and clustered using agglomerative hierarchical clustering with Ward’s linkage distance. (d) The L method is used to select the number of clusters from the dendrogram. (e) Each cluster is averaged and (f) within cluster variations are calculated using fPCA. Steps (b-f) are repeated for each of the three DOF arm models. Steps (b-d) are repeated once more for the 4 DOF shoulder-elbow model.

variables are required to reconstruct the upper-limb than Cartesian coordinates. A lower dimensional representation of arm motion is an important factor for calculating similarities while joint angle trajectories are easily interpretable and implementable prosthetic devices. The simplicity of the joint-angle system was therefore used through the rest the paper.

The analyzed upper-limb joint angle systems are based on 3 DOF wrist, 4 DOF elbow-wrist, and 7 DOF shoulder-elbow-wrist definitions according to [24], hereby referred to simply as 3 DOF, 4 DOF, and 7 DOF models, respectively. Additional analysis is performed on the 4 DOF shoulder-elbow as well. The shoulder angles consist of plane of elevation, angle of elevation [25], and internal axial rotation, using the second option for the humerus coordinate system in [24] as is detailed in Fig. 4. The elbow angle is formed using the forearm and humerus, while wrist angles include supination, wrist flexion, and ulnar deviation. For left-handed participants, the joint angles were inverted so that they are congruous to right-handed participants.

### B. Motion Segmentation

ADL tasks can be seen as composites of individual motion segments. Many quantitative approaches exist to human motion segmentation and are often based on analyzing various features of motion or use statistical and machine learning tools [26]–[29]. Ultimately, verification of segmentation is performed heuristically by comparing results to predefined ground truth. Therefore, instead of implementing an automatic segmentation technique, we manually defined the start and end points of each motion segment by identifying when the end effector reached zero velocity, when a food item was acquired (analogous to [30]), completed a transfer or task, or returned the object to the table or the hand to its ‘rest pose’ (Table 1).

### C. Divergence Measure

One challenge with comparing time-series data is the difference in duration. Linear resampling of the data fails at properly aligning the epochs, and divergences between motions would appear larger than they should. Modeling the data on the other hand, for example with polynomials, leads to a loss of information. Dynamic time warping (DTW) [31] works by resampling the time-series to equal in length while simultaneously minimizing the sum of square Euclidean distances, and given that the interest is in the kinematics of the arm and not the time component, this was an appropriate option. It works according to the following equation,

$$D(i, j) = \min \left\{ \begin{array}{l} D(i-1, j) + d(i, j) \\ D(i-1, j-1) + d(i, j) \\ D(i, j-1) + d(i, j) \end{array} \right\}, D(1, 1) = d(1, 1) \quad (1)$$

where  $d(i, j)$  corresponds to the Euclidean distance between the DOF of frame  $i$  of one motion segment and the DOF of frame  $j$  of the second motion segment. The optimal path is then calculated through matrix  $D(i, j)$  by starting at the last frames of each of the motions and moving backwards through the smallest distance values.

Because similar motions may be moving in opposite directions, such as bringing the cup to the mouth and returning

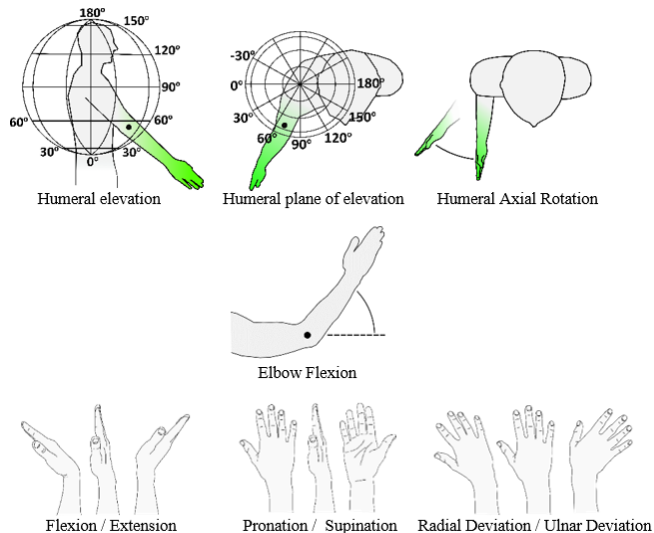


Fig. 4. Humeral elevation and plane of elevation are depicted using the globe system described in [22]. The elbow is positioned below the shoulder in the image to depict humeral axial rotation.

it to the table, it was necessary to calculate DTW twice, once with the original data and once with one of the motions moving in reverse; saving the smaller of the two calculations. Divergence values are normalized by dividing by the new time duration obtained during DTW. This is done so that the DTW comparison made between longer and shorter motions segments are comparable, and we refer to it as normalized-DTW. While this approach may bias longer segment comparisons, provided that the arm motion segments are on the same time scale this error is minimized. Although more robust DTW normalization methods exist, such as normalizing by the square root of the length [32], they did not significantly alter the results, and are therefore excluded from the analysis.

### D. Averaging Motions

Averaging of motions was performed during two separate phases throughout the analysis. The first time it was to average repetitions to obtain a single representative motion across participants; each final motion segment was an average of 36 motions (three from each participant). The second use of averaging was to identify a representative motion for each cluster. There are a variety of ways to computing a time-series average, the simplest one entails a linear resampling followed by a frame by frame averaging. DTW barycenter averaging (DBA) algorithm [33] is used instead, as it better handles phase shifts in the motions and epoch alignment.

One precaution that had to be made during DBA is that it is prone to local minimums, where the consensus segment will accentuate the amplitude of certain frames to minimize the DTW distance [33]. Although more complex algorithms exist that attempt to deal with such issues, such as [34], we simply limited the amount of frames that can be warped to the minimum amount possible when performing DTW between the shortest and the longest motion segment pair in each group.

### E. Agglomerative Hierarchical Clustering

In the present study we sought a clustering algorithm that effectively minimizes variation within clusters, maximizing the

difference between clusters, while depicting the underlying structure of the data. In order to further distinguish arm motions, the algorithm would ideally result in clusters that are “spherical” rather than interconnected. Agglomerative hierarchical clustering [35], [36] with Ward’s linkage criterion, or simply distance, accomplishes this while presenting the data in an easily interpretable dendrogram illustrating the distance relationship between the motion segments. The algorithm works by successively merging clusters based on a distance criterion until all but one cluster containing all of the data remains. Ward’s linkage criterion, unlike complete linkage (furthest-neighbor) or single linkage (nearest-neighbor), creates distinct “spherical” clusters by accounting for both the within and cumulative cluster variances according to

$$W = SS_{12} - (SS_1 + SS_2) \quad (2)$$

where  $W$  is the calculated Ward’s distance value,  $SS_{12}$  is the sum of squares of the combined cluster, and  $SS_1$  and  $SS_2$  are the sum of squares of each of the members of the cluster to its respective centroid. Although this method does not make adjustments to the clustering once a merge decision has been made, proper outlier and noise handling will mitigate this issue; we do so by averaging repetitions, outlined in Section D.

A set number of clusters can be extracted from the dendrograms in a variety of ways. While heuristics can be used to select a seemingly reasonable number of clusters for the 7 DOF model, the 4 DOF and 3 DOF models do not lend themselves to an easy interpretation. Therefore we use a data driven approach called the L method [37] to identify an “optimal” number of clusters. The method is used with a greedy evaluation approach, as recommended in [37], and only considers the Ward’s distance (2) value between the two clusters being merged. Unlike other approaches that only evaluate the data locally or are sensitive to noise, the L method makes use of the entire set of distance values between each merging pair to determine the point of transition, the “knee”, between the internally homogenous and non-homogenous cluster merging phases (Fig. 5). It works by linearly fitting each phase while varying the sequence of points that belong to each and calculating the total error,  $RMSE_{tot}$ , according to

$$RMSE_{tot} = \frac{c-1}{b-1} \times RMSE(L_c) + \frac{b-c}{b-1} \times RMSE(R_c) \quad (3)$$

where  $c$  and  $b$  correspond to the partitions of the distance data belonging to the left and right side, respectively, and  $L_c$  and  $R_c$  are the lines of best-fit, respectively.  $L_c$  and  $R_c$  must have at least two points, and  $c$  and  $b$  always add up to the total number of points. A value of  $c$  which minimizes  $RMSE_{tot}$  corresponds to the “optimal” number of clusters. Certain improvements to the L method were additionally recommended by the authors [37], and are implemented in the results. These include adjusting the number of mergings that are being evaluated and removing the set of data left of the point corresponding to the largest distance.

#### F. Cluster Quality

By re-computing the hierarchical clustering dendrogram using individual motions, rather than the average of each

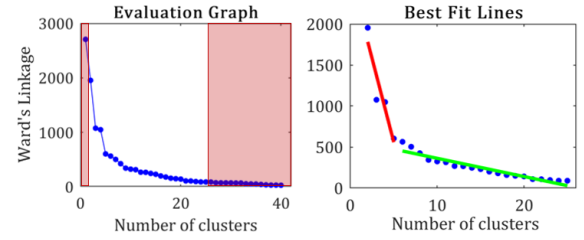


Fig. 5. Left plot depicts the suggested windowing of the merge distance data, as suggested in [37]. The right plot depicts an application of the L method; identifying the “knee” of the graph.

motion type, we can compute an evaluation score that captures how consistently repetitions cluster,

---

#### Algorithm 1 Compute Clustering Quality

---

**Input:** vector of cluster membership ID of each motion segment

**Output:** evaluation score as a %

```

1: Let max_score equal to 3060 // 12 subj.*85 motion segments *3 repetitions
2: Initialize score to 0
3: foreach cluster do
4:   foreach pair of cluster members do
5:     if cluster members are repetitions then add 1 to score
6:   end
7: end
8: return score / max_score * 100

```

---

The quality score is at its maximum for a single cluster containing all of the motion segments and decreases monotonically as the number of clusters increase. The evaluation score could theoretically remain at 100% up to 1020 clusters; 85 unique motions from 12 participants. Common clustering methods are additionally evaluated to validate the selection of the primary methodology: K-medoids clustering and Euclidean distance between motions represented using coefficients belonging to cubic Bézier fits.

K-medoids clustering is tested using DTW divergences, similar to [38]. Unlike K-means, K-medoids identifies a median motion segment instead of calculating a centroid. At each iteration, distances between representative cluster medians and the motion segments are calculated, cluster membership is reassigned, and new medians are computed. Ten repetitions of this algorithm were performed to account for local minimums.

An alternative divergence measure was tested; cubic Bézier curves were fit to each joint angle trajectory using least squares, yielding a set of Bézier control points that represented each motion segment. Cubic Béziers have been shown to accurately represent human motion during data compression [39] and hand trajectories [40]. One benefit to using Bézier curves over traditional polynomials is that the first and last control points correspond to the start and end locations of a trajectory. Cubic Bézier curves yielded feature vectors of 12, 16, and 28 elements long for the 3 DOF, 4 DOF, and 7 DOF models, respectively, corresponding to 4 control points. Euclidean distances between the feature vectors were calculated and Hierarchical clustering with Ward’s linkage criterion was then used for clustering.

#### G. Within Cluster Average and Variation

In order to obtain variation within each cluster, an average was first found, motions were resampled to be equal in duration, and fPCA [41] was used to extract the principal components (Fig. 6). Each set of the first  $n$  principal components then explains some amount of variation. Greater motion variability

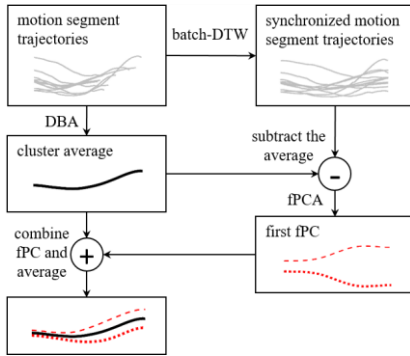


Fig. 6. Flowchart depicting the within cluster variation analysis pipeline. Top left panel represents the recorded motion segments belonging to a single cluster for one of the DOF, represented using joint angle trajectories.

will require more principal components to describe the same amount of variation than clusters with homogenous segments.

As described in section II. A., each motion within a cluster is an average of 36 individual motion segments, therefore a cluster with 2 motions can also be analyzed as a set of 72 individual motion segments. All of the individual motions that occur while replacing the object or returning the hand are first reversed. Then, as in section III. D., DBA is used to identify the average of each cluster, initializing it to have the same number of frames as the longest motion. The individual motions are then resampled to equal in length using batch-DTW [42]. Unlike linear resampling, batch-DTW is better suited for this application by aligning epochs independently for each motion, thus better capturing motion variability. Batch-DTW is an asymmetric DTW algorithm which simultaneously aligns multiple time-series data and retains a non-increasing time-duration, something that is impossible to achieve using standard DTW. It works by first selecting a reference time-series segment, in our case it is the average motion of a cluster, and performing DTW with each of the other time-series data. Each set of frames that are repeated for the reference segment, the other segment has those frames averaged instead. An example would be if the optimal warping path included  $(i-1, j)$ ,  $(i, j)$ ,  $(i+1, j)$ , where the  $(i-1)^{th}$ ,  $i^{th}$ , and  $(i+1)^{th}$  frames of motion  $M_i$  is aligned with the  $j^{th}$  frame of the reference motion  $M_j$ . Batch-DTW would take the following average of the three frames

$$(M_i(i-1, :) + M_i(i, :) + M_i(i+1, :)) / 3$$

Three 3<sup>rd</sup> order B-Spline [43] elements were fit to each of the newly aligned motion segments (using least squares). The coefficients of the curves are used as feature variables when calculating the principal components [41]. Since the motion alignment considers only the positions of the joint angles, velocity and acceleration information is lost, therefore instead of a 5<sup>th</sup> order fit as recommended in [44], 3<sup>rd</sup> order was chosen instead. Three equally spaced B-spline elements were primarily used to better capture the start, middle, and end phases of the joint angle trajectories.

#### IV. RESULTS

Fig. 7 displays dendrograms obtained for the joint angle 7 DOF full-arm model, 4 DOF elbow-wrist model, 3 DOF wrist-

only model, and the 4 DOF shoulder-elbow model. A horizontal cut is used to segment each of the dendrograms to obtain a subset of clusters according to the L method described in [37] using the greedy approach, whose results accompany the dendrograms in Fig. 8. The L method identified the following set of clusters: 5 clusters for the 3 DOF model, and 11 clusters for the rest. The shoulder-elbow trajectory dendrogram is nearly identical to the 7-DOF model barring two motions being placed in difference clusters, st-2 (transfer suitcase to table) and fr-2 (use fork).

One of the L method adjustments recommended by the authors [37] was to dynamically adjust the number of mergings being evaluated down to a minimum of 20 points. In our case, the identified “knee” for 25 merging points was equivalent and we therefore left the additional 5 points in. The largest merging distance for each DOF model was the first merging and therefore the data being evaluated started with the merging distance between 2 and 3 clusters.

Evaluation of the chosen methodology is shown against an alternative divergence measure and clustering algorithm while varying the number of clusters from 1 to 25 (Fig. 9). This was done for each DOF model. The chosen clustering methodology consistently outperforms the other methods for almost every number of clusters.

Due to practical limitations in representing multi-DOF motion with images or complex equations, we include all of the resulting average motions and the first two principal components of each cluster in the multi-media accompanying this paper. An example average motion representing the 8<sup>th</sup> cluster of the 7 DOF model, *reach-to-front-far*, is shown in Fig. 10, in which the start, middle, and end poses of the arm are displayed. The location of the end effector is also traced out throughout the motion. The stick model is created using forward kinematics of the average motion’s DOF in MATLAB (MathWorks, US) according to [24], and the accompanying skeleton model was created using an online skeletal animation tool, KineMan (<http://www.kineman.com>). The first principal component for each DOF of the motion is also included in the figure. Start and end locations of the average of the 4<sup>th</sup> cluster from the wrist model, *supination + flexion*, are additionally shown in Fig. 11. The motions for the wrist and elbow-wrist models were depicted using only the KineMan tool.

Variation of the motions within each cluster is captured using fPCA. The percent of the variability explained by each set of principal components, i.e. the first  $n$  number of principal components, is summarized in Fig. 12. For each cluster the average pair-wise divergence between cluster members is additionally included, calculated using normalized-DTW. The analysis indicated that while some clusters needed only 3 principal components to describe 80% of the variation, others needed as many as 8.

#### V. DISCUSSION

Although the hierarchical tree does not output a specific number of clusters, clustered groups can be obtained by transecting the dendrogram at a desired value. The most straightforward method is using a straight line cut as is seen in

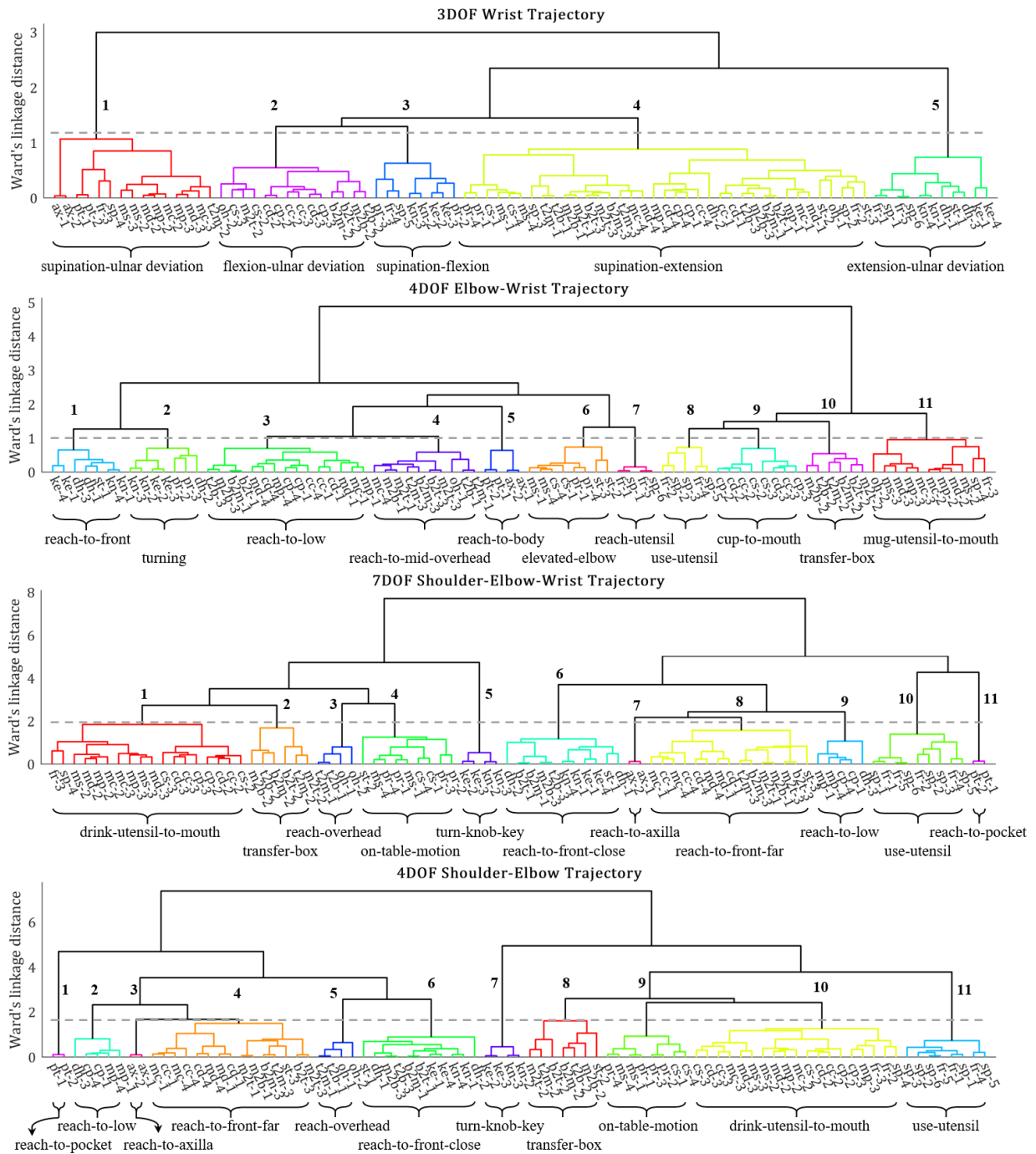


Fig. 7. Dendrograms for the 3, 4, and 7 DOF models. Location of the horizontal cut (dashed line) was chosen using results of the L method. An appropriate cluster name accompanies each of the clusters: major axes of wrist rotation for the 3 DOF model and generalized description of the motions for the 4 and 7 DOF models. Cluster colors are auto-generated and are unrelated between dendrograms.

Fig. 7. The location of this cut was chosen using a data driven approach called the L method with greedy evaluation, chosen over global primarily due to greater reliability when selecting the number of clusters [37]. Global evaluations have shown only minor deviations and were not considered in the analysis.

According to the L method, unlike for the 4 DOF elbow-wrist model, 7 DOF and 3 DOF models have a clear RMSE minimum suggesting 11 and 5 clusters, respectively. Clusters obtained for the 7 DOF model, similar to results found in our previous work [23] and consistent with the spatial control hypothesis [45], can

be estimated using hand start and end locations while smaller groupings within each cluster are based on other movement characteristics. This suggests that either the wrist motion is synergistic with the shoulder and elbow joints along the motion path [7], [46], or that its range of motion was not significant enough to influence clustering. Depending on the set of motions being studied, it is likely that both are factors. To test this we analyzed the shoulder-elbow trajectories, which identified nearly identical clusters to the 7 DOF model, further suggesting that arm motions primarily clustered according to task location.

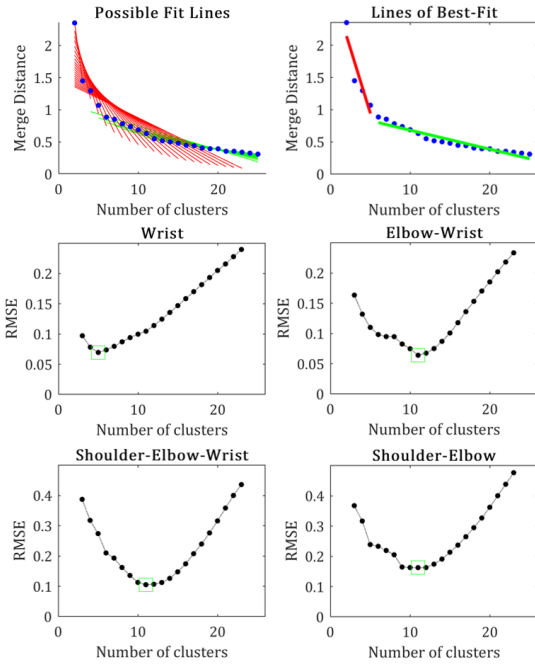


Fig. 8. L method results for each of the models. An example of the identified “knee” for the Wrist model is included at the top row.

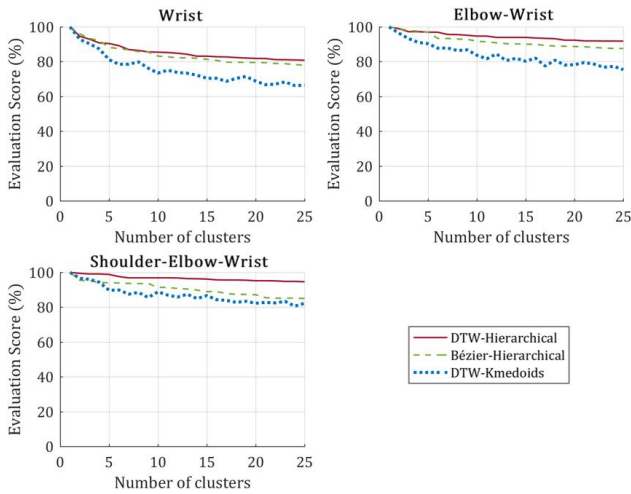


Fig. 9. Quality of clustering for different divergence measures and clustering algorithms across a range of number of clusters. Scoring metric assessed how frequently repetitions from the same individuals clustered together.

Therefore when designing a 7 DOF prosthetic device control scheme, priority should be given to the location of the end effector. The 3 DOF model too created clusters primarily based on starts and ends of the wrist joint angle trajectories.

Although the global minimum is located at 11 clusters, the 4 DOF elbow-wrist model has an additional RMSE minimum at 6 clusters, indicating the possibility of a second plausible interpretation: clustering result for the 4 DOF model is not a gradual transition between the 7 DOF and 3 DOF models, but rather it exhibits both of their minimums simultaneously. We therefore suspect that 11 and 6 cluster minimums correspond to hand location and wrist orientation, respectively. Although the dendrogram structure for the 4 DOF model is more difficult to interpret, given that 11 clusters were ultimately identified despite the absence of shoulder angles, it would appear that task location information is largely maintained in the elbow

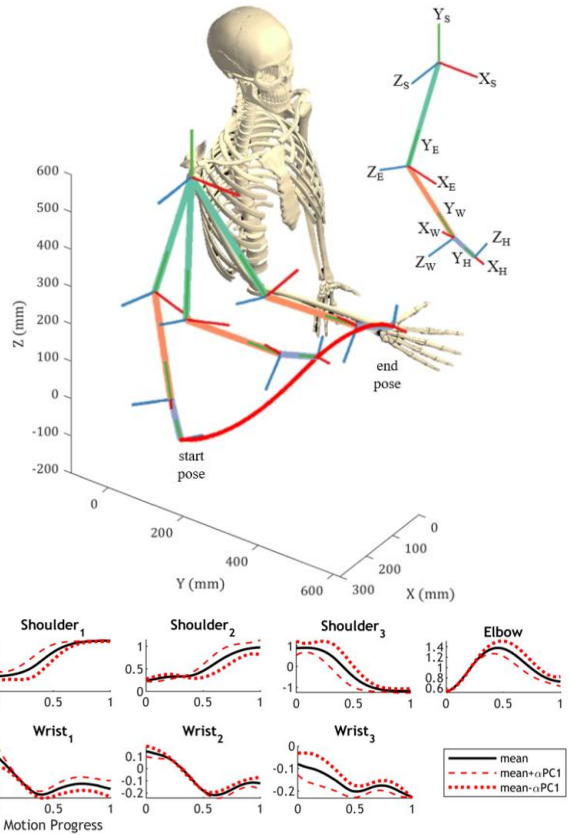


Fig. 10. Forward kinematics are used to display the average motion of the 8<sup>th</sup> cluster for the 7 DOF model, *reach-to-front-far*. Three reference frames are displayed with X, Y, and Z axis using subscripts S, E, W, and H for shoulder, elbow, wrist, and hand, respectively. The shoulder coordinate frame is fixed throughout the motion. Humerus, forearm, and hand lengths correspond to an average adult. DOF angle correspond, respectively, to humeral elevation, plane of elevation, internal rotation, elbow flexion, wrist supination, wrist flexion, and wrist deviation. Individual joint angle trajectories are displayed along with the first principal component.  $\alpha$  was set to equal the proportion of total variation explained by that component.

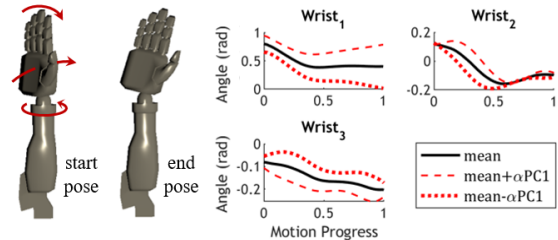


Fig. 11. Start and end poses of the 4<sup>th</sup> cluster for the 3 DOF model, *supination+flexion*, are shown on the left along with the joint angle trajectories and the first principal component on the right. The three joint angles in order correspond to supination, flexion, and deviation.  $\alpha$  was set to equal the proportion of total variation explained by the principal component. Red arrows indicate the general direction of motion for each of the DOF.

trajectory, consistent with the efforts in [7].

3 DOF clusters are summarized as motions types, such as supination or deviation, referring to the most significant degree(s) of freedom. The dart-throwing motion (DTM), a hybrid of flexion and ulnar deviation, which has been described as a more stable and controllable axis of rotation [47], is re-discovered in our analysis as the average of the 2<sup>nd</sup> cluster. Since dendrogram interpretation is limited without animation, and while cluster descriptions for all three models are generalized in Fig. 7, readers are urged to view the average motions in the

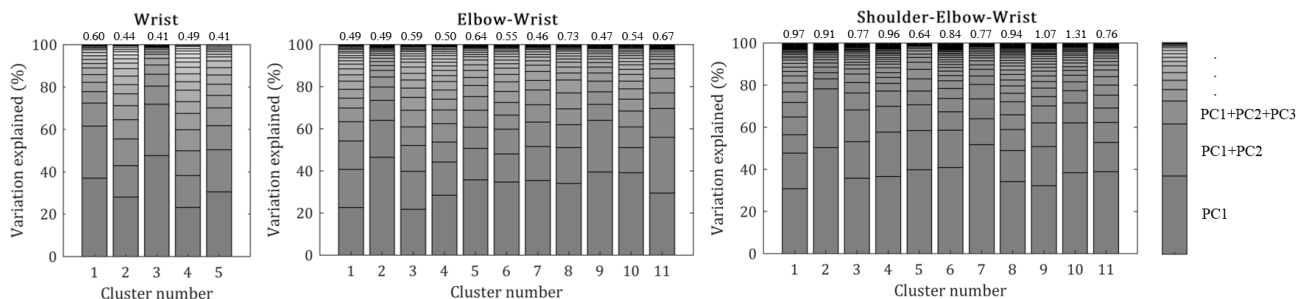


Fig. 12. The variation explained by each set of principal components for each joint angle system’s averages are displayed. Note that clusters requiring more principal components to explain the same amount of variation is generally consistent with a greater amount of motions they represent. Average pair-wise divergence is included at the top of each bar.

multi-media that accompanies this paper.

The chosen divergence measure and clustering algorithm outperformed Bézier and K-medoids methods at almost every number of clusters, reassuring its selection. The performance of K-medoids did not monotonically decrease with added clusters due to the algorithm reaching local minimums despite multiple iterations. Using Bézier coefficients to measure similarities between motions performed worse than DTW likely due to Bézier coefficients merely approximating the data whereas DTW takes the full joint angle trajectories into account and thus calculates a more representative divergence value.

Average pair-wise divergence and fPCA analysis capture the spread of a cluster and the directions of that spread, respectively. Although some clusters require as many as 8 fPC’s to describe 80% of the variation, if the average pair-wise divergence is small, this does not necessarily mean that all of those fPC’s are required to accurately reconstruct the motions for practical use in a prosthetic device. The torso could potentially compensate for the variation as well.

The demonstrated cluster average in Fig. 10 and Fig. 11 can be directly implemented in a semi-autonomous robotic or prosthetic upper-limb model. The accompanying principal components in the same figures indicate how these motions vary, but can also be used to inform how to dynamically tune the trajectory to compensate for the motion variation within the cluster. This may be an indispensable aspect of control when, for example, reaching locations occur in continuous space. Future work should take advantage of fPCA findings in implementation of motion control and online adjustments.

If a common set of feature variables is identified, comparison may potentially be made with cyclical motions as well. One challenge is that cyclical motions do not have well defined start and end points, and therefore rely on alternative representation methods such as wavelet or discrete Fourier transform [48]. However, these methods would not be appropriate for the non-cyclical type of data considered thus far in this study.

The decision to use joint angle data as the feature vector largely relied on the ability of recorded motions to be easily interpreted across individuals and its low dimensional representation. However, this choice suffers from giving each joint angle an equal weight when calculating the divergence between motions, while it may have been less of an issue for Cartesian coordinates of the upper-limb segments. Additionally, proximity to the discontinuities in two of the shoulder joint angles may cause them to have a larger impact when measuring

motion similarity since the angle range is likely to be greater than for the other joint angles. Alternative arm features have been proposed in the literature, such as the arm triangle [49], or defining a new angle eliminating one of the discontinuities [50], either of which could be used in future iterations. Finally, although the decision to analyze the 3, 4, and 7 DOF arm models is relevant in a variety of applications, the methodology can be extended to alternative systems, such as to a full body kinematic chain.

## VI. CONCLUSION AND FUTURE WORK

This paper described a method that categorizes human arm motion during the performance of ADL tasks. Using data driven techniques to measure similarity between motions, average, and cluster, 11 motion categories were identified for the 7 DOF arm and 4 DOF elbow-wrist models and 5 motion categories for the 3 DOF wrist model. These clusters can be distinguished primarily based on start and end configurations of motions, further differentiated by specific types of manipulation.

The results align with intuition as well, making the proposed method a good candidate to describe other DOF time-series systems. The application of this work is not task specific and is not exhaustive of the full set and complexity of motions within each task category, but instead provides a general framework that may be either applied in its current form for general use, improved on using fPCA, or could further be adapted to task specific scenarios to increase motion specificity. An example includes obtaining a partial hierarchy of motions exclusively for feeding [30]. The proposed approach could also be applied to a subset of the presented data, such as decoupling the reaching location from the wrist orientation. Future developments include testing and verifying the identified average motions, implementation of a dynamic control of the average motions according to fPCA results, and identifying the role the torso plays during similar ADL tasks at different locations with respect to a fixed body frame.

## REFERENCES

- [1] C. J. van Andel, N. Wolterbeek, C. A. M. Doorenbosch, D. J. (H. E. J. ). Veeger, and J. Harlaar, “Complete 3D kinematics of upper extremity functional tasks,” *Gait Posture*, vol. 27, no. 1, pp. 120–127, 2008.
- [2] A. M. Oosterwijk, M. K. Nieuwenhuis, C. P. van der Schans, and L. J. Mouton, “Shoulder and elbow range of motion for the performance of activities of daily living: A systematic review,” *Physiother. Theory Pract.*, vol. 34, no. 7, pp. 505–528, 2018.
- [3] T. Kang, J. He, and S. I. H. Tillery, “Determining natural arm

- configuration along a reaching trajectory.," *Exp. Brain Res.*, vol. 167, no. 3, pp. 352–361, 2005.
- [4] A. Spiers, S. G. Khan, and G. Herrmann, *Biologically Inspired Control of Humanoid Robot Arms: Robust and Adaptive Approaches*, 1st ed. Springer International Publishing, 2016.
- [5] A. Fougner, Ø. Stavadahl, P. J. Kyberd, Y. G. Losier, and P. A. Parker, "Control of Upper Limb Prostheses: Terminology and Proportional Myoelectric Control — A Review," *IEEE Trans. Neural Syst. Rehabil. Eng.*, vol. 20, no. 5, pp. 663–677, 2012.
- [6] M. Merad, A. Roby-Brami, and N. Jarrasse, "Towards the implementation of natural prosthetic elbow motion using upper limb joint coordination," in *International Conference on Biomedical Robotics and Biomechatronics*, 2016, pp. 821–826.
- [7] R. R. Kaliki, R. Davoodi, and G. E. Loeb, "Prediction of Distal Arm Posture in 3-D Space From Shoulder Movements for Control of Upper Limb Prostheses," *Proc. IEEE*, vol. 96, no. 7, pp. 1217–1225, 2008.
- [8] L. Resnik *et al.*, "Development and Evaluation of the Activities Measure for Upper Limb Amputees," *Arch. Phys. Med. Rehabil.*, vol. 94, no. 3, pp. 488–494, 2013.
- [9] C. S. Chung, H. Wang, and R. A. Cooper, "Functional assessment and performance evaluation for assistive robotic manipulators: Literature review," *J. Spinal Cord Med.*, vol. 36, no. 4, pp. 273–289, 2013.
- [10] E. Biddiss and T. Chau, "Upper limb prosthesis use and abandonment: A survey of the last 25 years," *Prosthetics and Orthotics International*, vol. 31, no. 3, pp. 236–257, 2007.
- [11] F. Cordella *et al.*, "Literature review on needs of upper limb prosthesis users," *Front. Neurosci.*, vol. 10, pp. 1–14, 2016.
- [12] C. Wang *et al.*, "Kinematic Redundancy Analysis during Goal-Directed Motion for Trajectory Planning of an Upper-Limb Exoskeleton Robot," in *Proceedings of the Annual International Conference of the IEEE Engineering in Medicine and Biology Society*, 2019, pp. 5251–5255.
- [13] D. Farina *et al.*, "The Extraction of Neural Information from the Surface EMG for the Control of Upper-Limb Prostheses: Emerging Avenues and Challenges," *Trans. Neural Syst. Rehabil. Eng.*, vol. 22, no. 4, pp. 797–809, 2014.
- [14] L. Bi, A. Feleke, and C. Guan, "A review on EMG-based motor intention prediction of continuous human upper limb motion for human-robot collaboration," *Biomed. Signal Process. Control*, vol. 51, pp. 113–127, 2019.
- [15] P. K. Artemiadis and K. J. Kyriakopoulos, "EMG-Based Control of a Robot Arm Using Low-Dimensional Embeddings," *Trans. Robot.*, vol. 26, no. 2, pp. 393–398, 2010.
- [16] C. L. Pulliam, J. M. Lambrecht, and R. F. Kirsch, "EMG-Based Neural Network Control of Transhumeral Prostheses," *J. Rehabil. Res. Dev.*, vol. 48, no. 6, pp. 739–754, 2013.
- [17] G. Averta, C. Della Santina, E. Battaglia, F. Felici, M. Bianchi, and A. Bicchi, "Unveiling the Principal Modes of Human Upper Limb Movements," *Front. Robot. AI*, vol. 4, no. 37, pp. 1–12, 2017.
- [18] S. Sheikholeslami, G. Lee, J. W. Hart, S. Srinivasa, and E. A. Croft, "A Study of Reaching Motions for Collaborative Human-Robot Interaction," in *International Symposium on Experimental Robotics*, 2018, pp. 584–594.
- [19] T. M. Tuan, P. Souères, M. Taïx, M. N. Sreenivasa, and C. Halgand, "Humanoid human-like reaching control based on movement primitives," in *Proceedings - IEEE International Workshop on Robot and Human Interactive Communication*, 2010, pp. 546–551.
- [20] D. Kulić, W. Takano, and Y. Nakamura, "Online segmentation and clustering from continuous observation of whole body motions," *IEEE Trans. Robot.*, vol. 25, no. 5, pp. 1158–1166, 2009.
- [21] D. H. Gates, L. S. Walters, J. Cowley, J. M. Wilken, and L. Resnik, "Range of Motion Requirements for Upper-Limb Activities of Daily Living," *Am. J. Occup. Ther.*, vol. 70, no. 1, 2016.
- [22] D. J. Magermans, E. K. J. Chadwick, H. E. J. Veeger, and F. C. T. van der Helm, "Requirements for upper extremity motions during activities of daily living," *Clin. Biomech.*, vol. 20, no. 6, pp. 591–599, 2005.
- [23] Y. Gloumakov, A. J. Spiers, and A. M. Dollar, "A Clustering Approach to Categorizing 7 Degree-of-Freedom Arm Motions during Activities of Daily Living," in *IEEE International Conference on Robotics and Automation*, 2019.
- [24] G. Wu *et al.*, "ISB recommendation on definitions of joint coordinate systems of various joints for the reporting of human joint motion — Part II: shoulder, elbow, wrist and hand," *J. Biomech.*, vol. 38, no. 5, pp. 981–992, 2005.
- [25] C. A. M. Doorenbosch, J. Harlaar, and D. Veeger, "The globe system: An unambiguous description of shoulder positions in daily life movements," *J. Rehabil. Res. Dev.*, vol. 40, no. 2, p. 147, 2003.
- [26] J. Barbic, A. Safonova, J.-Y. Pan, C. Faloutsos, J. K. Hodgins, and N. S. Pollard, "Segmenting Motion Capture Data into Distinct Behaviors," in *Proceedings of Graphics Interface*, 2004, pp. 185–194.
- [27] D. Kulić, C. Ott, D. Lee, J. Ishikawa, and Y. Nakamura, "Incremental learning of full body motion primitives and their sequencing through human motion observation," *Int. J. Rob. Res.*, vol. 31, no. 3, pp. 330–345, 2011.
- [28] G. Xia, H. Sun, L. Feng, G. Zhang, and Y. Liu, "Human Motion Segmentation via Robust Kernel Sparse Subspace Clustering," *Trans. Image Process.*, vol. 27, no. 1, pp. 135–150, 2018.
- [29] X. Zan, W. Liu, and W. Xing, "A framework for human motion segmentation based on multiple information of motion data," *Trans. Internet Inf. Syst.*, vol. 13, no. 9, pp. 4624–4644, 2019.
- [30] T. Bhattacharjee, G. Lee, H. Song, and S. S. Srinivasa, "Towards Robotic Feeding: Role of Haptics in Fork-Based Food Manipulation," *IEEE Robot. Autom. Lett.*, vol. 4, no. 2, pp. 1485–1492, 2019.
- [31] H. Sakoe and S. Chiba, "Dynamic Programming Algorithm Optimization for Spoken Word Recognition," *IEEE Trans. Acoust.*, vol. 26, no. 1, pp. 43–49, 1978.
- [32] M. Linardi, Y. Zhu, T. Palpanas, and E. Keogh, "Matrix profile X: VALMOD-scalable discovery of variable-length motifs in data series," *Proc. ACM SIGMOD Int. Conf. Manag. Data*, pp. 1053–1066, 2018.
- [33] F. Petitjean, A. Ketterlin, and P. Gancarski, "A global averaging method for dynamic time warping, with applications to clustering," *Pattern Recognit.*, vol. 44, no. 3, pp. 678–693, 2011.
- [34] M. Cuturi and M. Blondel, "Soft-DTW: a Differentiable Loss Function for Time-Series," in *Proceedings of the 34th International Conference on Machine Learning*, 2017.
- [35] B. S. Everitt, S. Landau, M. Leese, and D. Stahl, *Cluster Analysis*, 5th ed. West Sussex, U.K.: John Wiley & Sons, 2011.
- [36] A. Saxena *et al.*, "A review of clustering techniques and developments," *Neurocomputing*, vol. 267, pp. 664–681, 2017.
- [37] S. Salvador and P. Chan, "Determining the Number of Clusters/Segments in Hierarchical Clustering/Segmentation Algorithms," in *International Conference on Tools with Artificial Intelligence*, 2004.
- [38] V. T. Huy and D. T. Anh, "An efficient implementation of anytime K-medoids clustering for time series under dynamic time warping," *ACM Int. Conf. Proceeding Ser.*, vol. 08-09-Dece, pp. 22–29, 2016.
- [39] O. Arıkan, "Compression of Motion Capture Databases," *ACM Trans. Graph.*, vol. 25, no. 3, pp. 890–897, 2006.
- [40] J. J. Faraway, M. P. Reed, and J. Wang, "Modelling three-dimensional trajectories by using Bezier curves with application to hand motion," *J. R. Stat. Soc. Ser. C Appl. Stat.*, vol. 56, no. 5, pp. 571–585, 2007.
- [41] J. Ramsay and B. W. Silverman, *Functional Data Analysis*, 2nd ed. Springer-Verlag New York, 2005.
- [42] A. Kassidas, J. F. Macgregor, and P. A. Taylor, "Synchronization of Batch Trajectories Using Dynamic Time Warping," *Am. Inst. Chem. Eng.*, vol. 44, no. 4, pp. 864–875, 1998.
- [43] C. de Boor, *A Practical Guide to Splines*, 1st ed. Springer-Verlag New York, 1978.
- [44] T. Flash and N. Hogans, "The coordination of arm movements: an experimentally confirmed mathematical model," *J. Neurosci.*, vol. 5, no. 7, pp. 1688–1703, 1985.
- [45] P. Morasso, "Spatial Control of Arm Movements," *Exp. Brain Res.*, vol. 42, pp. 223–227, 1981.
- [46] F. Montagnani, M. Controzzi, and C. Cipriani, "Exploiting arm posture synergies in activities of daily living to control the wrist rotation in upper limb prostheses: A feasibility study," in *Proceedings of the 2015 International Conference of the IEEE Engineering in Medicine and Biology Society*, 2015, pp. 2462–2465.
- [47] H. Moritomo, E. P. Apergis, G. Herzberg, F. W. Werner, S. W. Wolfe, and M. Garcia-Elias, "2007 IFSSH Committee Report of Wrist Biomechanics Committee: Biomechanics of the So-Called Dart-Throwing Motion of the Wrist," *J. Hand Surg. Am.*, vol. 32, no. 9, pp. 1447–1453, 2007.
- [48] S. Aghabozorgi, A. Seyed, and T. Y. Wah, "Time-series clustering – A decade review," *Inf. Syst.*, vol. 53, pp. 16–38, 2015.
- [49] C. Fang and X. Ding, "A Set of Basic Movement Primitives for Anthropomorphic Arms," in *IEEE International Conference on Mechatronics and Automation*, 2013, pp. 639–644.
- [50] T. Masuda, A. Ishida, L. Cao, and S. Morita, "A proposal for a new definition of the axial rotation angle of the shoulder joint," *J. Electromyogr. Kinesiol.*, vol. 18, no. 1, pp. 154–159, 2008.